Available online at www.sciencedirect.com
SCIENCE DIRECT
Geochimica et Cosmochimica Acta 70 (2006) 206–223
Geochimica
www.elsevier.com/locate/gca

Vapor pressures and evaporation coefficients for melts of ferromagnesian chondrule-like compositions

A.V. Fedkin [a,*], L. Grossman [a,b], M.S. Ghiorso [a]

[a] Department of the Geophysical Sciences, The University of Chicago, 5734 South Ellis Avenue, Chicago, IL 60637, USA
[b] Enrico Fermi Institute, The University of Chicago, 5640 South Ellis Avenue, Chicago, IL 60637, USA

Received 9 May 2005; accepted in revised form 17 August 2005

Abstract

To determine evaporation coefficients for the major gaseous species that evaporate from silicate melts, the Hertz–Knudsen equation was used to model the compositions of residues of chondrule analogs produced by evaporation in vacuum by Hashimoto [Hashimoto A. (1983) Evaporation metamorphism in the early solar nebula-evaporation experiments on the melt FeO–MgO–SiO_2–CaO–Al_2O_3 and chemical fractionations of primitive materials. *Geochem. J.* 17, 111–145] and Wang et al. [Wang J., Davis A. M., Clayton R. N., Mayeda T. K., Hashimoto A. (2001) Chemical and isotopic fractionation during the evaporation of the FeO–MgO–SiO_2–CaO–Al_2O_3–TiO_2 rare earth element melt system. *Geochim. Cosmochim. Acta* 65, 479–494], in vacuum and in H_2 by Yu et al. [Yu Y., Hewins R. H., Alexander C. M. O'D., Wang J. (2003) Experimental study of evaporation and isotopic mass fractionation of potassium in silicate melts. *Geochim. Cosmochim. Acta* 67, 773–786], and in H_2 by Cohen et al. [Cohen B. A., Hewins R. H., Alexander C. M. O'D. (2004) The formation of chondrules by open-system melting of nebular condensates. *Geochim. Cosmochim. Acta* 68, 1661–1675]. Vapor pressures were calculated using the thermodynamic model of Ghiorso and Sack [Ghiorso M. S., Sack R. O. (1995) Chemical mass transfer in magmatic processes IV. A revised and internally consistent thermodynamic model for the interpolation and extrapolation of liquid–solid equilibria in magmatic systems at elevated temperatures and pressures. *Contrib. Mineral. Petrol.* 119, 197–212], except for the late, FeO-free stages of the Wang et al. (2001) and Cohen et al. (2004) experiments, where the CMAS activity model of Berman [Berman R. G. (1983) A thermodynamic model for multicomponent melts, with application to the system CaO–MgO–Al_2O_3–SiO_2. Ph.D. thesis, University of British Columbia] was used. From these vapor pressures, evaporation coefficients (α) were obtained that give the best fits to the time variation of the residue compositions. Evaporation coefficients derived for $Fe_{(g)}$, $Mg_{(g)}$, and $SiO_{(g)}$ from the Hashimoto (1983) experiments are similar to those found by Alexander [Alexander C. M. O'D. (2004) Erratum. *Meteoritics Planet. Sci.* 39, 163] in his EQR treatment of the same data and also adequately describe the FeO-bearing stages of the Wang et al. (2001) experiments. From the Yu et al. (2003) experiments at 1723 K, $\alpha_{Na} = 0.26 \pm 0.05$, and $\alpha_K = 0.13 \pm 0.02$ in vacuum, and $\alpha_{Na} = 0.042 \pm 0.020$, and $\alpha_K = 0.017 \pm 0.002$ in 9×10^{-5} bar H_2. In the FeO-free stages of the Wang et al. (2001) experiments, α_{Mg} and α_{SiO} are significantly different from their respective values in the FeO-bearing portions of the same experiments and from the vacuum values obtained at the same temperature by Richter [Richter F. M., Davis A. M., Ebel D. S., Hashimoto A. (2002) Elemental and isotopic fractionation of Type B calcium-, aluminum-rich inclusions: experiments, theoretical considerations, and constraints on their thermal evolution. *Geochim. Cosmochim. Acta* 66, 521–540] for CMAS compositions much lower in MgO. When corrected for temperature, the values of α_{Mg} and α_{SiO} that best describe the FeO-free stages of the Wang et al. (2001) experiments also adequately describe the FeO-free stage of the Cohen et al. (2004) H_2 experiments, but α_{Fe} that best describes the FeO-bearing stage of the latter experiment differs significantly from the temperature-corrected value derived from the Hashimoto (1983) vacuum data.

1. Introduction

Chondrules formed in the solar nebula by melting of solid precursors. At the peak temperatures experienced by molten chondrules, 1673–2123 K (Hewins et al., 2005),

* Corresponding author. Fax: +1 773 702 9505.
E-mail address: avf@uchicago.edu (A.V. Fedkin).

0016-7037/$ - see front matter © 2005 Elsevier Inc. All rights reserved.
doi:10.1016/j.gca.2005.08.014

equilibrium vapor pressures of many major and minor elements are thought to be sufficiently high that significant fractions of them would have evaporated. Studies of chondrules show, however, that they contain appreciable concentrations of alkalies (e.g., Jones, 1990, 1994) and only small to non-existent heavy isotope enrichments in Fe (Alexander and Wang, 2001) and K (Alexander et al., 2000), implying that their bulk chemical compositions have been largely unaffected by evaporation. Possible explanations may be that the equilibrium vapor pressures over silicate melts of these compositions are lower than anticipated; or that, despite high equilibrium vapor pressures, evaporation rates are low because evaporation coefficients are low; or that, despite sufficiently high vapor pressures and evaporation rates, the fraction of evaporated material was low due to some aspect of the physico-chemical conditions, such as thermal history and/or ambient gas composition. Heating experiments conducted on molten chondrule analogs show that significant evaporative losses of alkalies, Fe, Mg, and Si occur on time-scales of minutes to hours, suggesting that the absence of such effects in natural chondrules is indeed related to the conditions of evaporation. Modeling chondrule evaporation is one way of determining the conditions necessary for retarding this process. To be successful, such models require equilibrium vapor pressures of the dominant species that evaporate from melts of chondrule compositions, and evaporation coefficients for those species in appropriate ambient gas compositions.

Isothermal evaporation experiments have been performed on chondrule analog compositions in vacuum or at low pressures of hydrogen by several workers. When appropriate thermodynamic models are used to describe the condensed phase assemblages in these experiments, equilibrium vapor pressures can be calculated which, when combined with evaporation rates measured in these experiments, can be used to determine the evaporation coefficients. Just such an approach was used to obtain evaporation coefficients in $CaO–MgO–Al_2O_3–SiO_2$ (CMAS) liquids by Grossman et al. (2000), using the Berman (1983) activity–composition relations for such systems. The presence of additional components, such as FeO, Na_2O, and K_2O, in chondrules requires use of the more comprehensive thermodynamic model, MELTS, of Ghiorso and Sack (1995). In fact, Alexander (2002, 2004) and Ebel (2005) obtained evaporation coefficients by applying the MELTS model to some of the same experiments discussed herein. Alexander did not discuss the dependence of vapor pressures on bulk composition and oxygen fugacity, f_{O_2}, nor did he consider the interdependence of f_{O_2} and Fe^{3+}/Fe^{2+} ratio. In his work, Ebel (2005) assumed that no Fe^{3+} was present, so he was unable to constrain f_{O_2} with the Fe^{3+}/Fe^{2+} ratio. In this work, application of the MELTS thermodynamic model to the experiments of Hashimoto (1983), Cohen et al. (2004), Wang et al. (2001), and Yu et al. (2003) is used to study the variation of the vapor pressures of $Mg_{(g)}$, $Fe_{(g)}$, $FeO_{(g)}$, $SiO_{(g)}$, $Na_{(g)}$, and $K_{(g)}$ as a function of temperature, bulk composition, and oxygen fugacity, and to obtain evaporation coefficients for these species. A preliminary version of this work was presented by Fedkin et al. (2005).

2. Technique

2.1. Vapor pressure calculation

In laboratory evaporation experiments on chondrule-like compositions, a gas of known composition and pressure flows through a furnace or a furnace is evacuated. A solid assemblage of known composition is placed inside the furnace where it is heated to a temperature at which it melts into a droplet, which may or may not contain crystals. The driving force for evaporation is the difference in chemical potential of a component between the droplet and the ambient gas. In this work, chemical potentials in the droplet are represented by equilibrium vapor pressures at the droplet surface computed from them, even though these vapor pressures are never realized in these continuously evacuated experiments. For each element i, an equation is written in which the sum of the partial pressures of all species of element i, multiplied by their respective stoichiometric coefficients, is defined as P_i^{tot}. When the number of moles per unit volume is fixed at a given temperature, such relations become mass-balance equations. Examples are shown for H, Si, and Na in Eqs. (1)–(3), respectively.

$$P_{\text{H}} + 2P_{\text{H}_2\text{O}} + 3P_{\text{NH}_3} + 4P_{\text{CH}_4} + \cdots = P_{\text{H}}^{\text{tot}}, \tag{1}$$

$$P_{\text{SiO}} + P_{\text{SiO}_2} + \cdots = P_{\text{Si}}^{\text{tot}}, \tag{2}$$

$$P_{\text{Na}} + P_{\text{NaOH}} + \cdots = P_{\text{Na}}^{\text{tot}}. \tag{3}$$

After evaporation begins, there may be two contributors to the total pressure of any element i, an amount originally present in the gas and an amount derived by evaporation. This can be expressed as

$$P_i^{\text{tot}} = P_i^{\text{gas}} + P_i^{\text{drop}}, \tag{4}$$

where P_i^{gas} is the total initial, pre-evaporation pressure of element i, and P_i^{drop} is the evaporative contribution to the total pressure of element i. Some elements, such as H, C, and N, are treated as always being entirely in the gas phase during the experiment. For these, $P_i^{\text{drop}} = 0$ and $P_i^{\text{tot}} = P_i^{\text{gas}}$. Other elements, such as Mg, Si, and Na, are entirely derived from the droplet. For these elements, $P_i^{\text{gas}} = 0$ and $P_i^{\text{tot}} = P_i^{\text{drop}}$.

The equations for elements present only in the gas phase can be rewritten as in the following case of Eq. (1) for hydrogen

$$P_{\text{H}} + 2K_1P_{\text{H}}^2P_{\text{O}} + 3K_2P_{\text{N}}P_{\text{H}}^3 + 4K_3P_{\text{C}}P_{\text{H}}^4 + \cdots = P_{\text{H}}^{\text{gas}}, \tag{5}$$

where K_1, K_2, and K_3 are the equilibrium constants for formation of $H_2O_{(g)}$, $NH_{3(g)}$, and $CH_{4(g)}$, respectively, from their monatomic gaseous constituent elements. The identities of the 85 gaseous species carried in the calculation are

given in Table 1. Sources for their thermodynamic data are given in Ebel and Grossman (2000).

For each element present in the condensed phase, except for oxygen, the fugacity of each species is equated to its vapor pressure in the mass-balance equation for that element. Thus, Eq. (2) for Si becomes

$$\frac{K_7 a_{SiO_2}}{P_O} + K_8 a_{SiO_2} + \cdots = P_{Si}^{drop}, \tag{6}$$

where K_7 and K_8 are the equilibrium constants for the volatilization reactions,

$$SiO_{2(l)} \Longleftrightarrow SiO_{(g)} + O_{(g)} \tag{7}$$

and

$$SiO_{2(l)} \Longleftrightarrow SiO_{(g)}, \tag{8}$$

respectively, a_{SiO_2} is the activity of SiO_2 in the liquid, and P_O is the partial pressure of monatomic oxygen. Such substitutions effectively equilibrate each component of the condensed phase with the gas. Given the temperature and bulk chemical composition of the condensed part of the system, the MELTS computer code of Ghiorso and Sack (1995) is used to determine the identities and compositions of the equilibrium phases present, their molar proportions, densities, and volume proportions, as well as the activities of all components in the liquid fraction. Given the f_{O_2}, MELTS also determines the distribution of iron among its oxidation states.

Some MELTS liquid components contain more than one metal. For each of these components, Mg_2SiO_4, Fe_2SiO_4, $MgCr_2O_4$, $CaSiO_3$, Na_2SiO_3, and $KAlSiO_4$, evaporation reactions are written to produce the vapor species of one metal and one or more different liquid components of the other(s). Thus, Eq. (3) for Na becomes

Table 1
Gas species included in the calculation

Ar	AlOH	$Ca(OH)_2$	HCN
H	AlH	Na	O_2
O	AlO_2H	NaO	CO
C	Al_2O_2	Na_2	CO_2
N		NaOH	N_2
Si	Cr	NaH	NO
SiO	CrO	$(NaOH)_2$	CH
SiO_2	CrO_2	NaCN	CH_2
SiH	CrO_3	$(NaCN)_2$	CH_3
Si_2	CrN	K	CH_4
Si_2C	Fe	K_2	CN
SiC_2	FeO	KO	C_2
SiH_4	$Fe(OH)_2$	KOH	C_2H
SiN	Mg	$(KOH)_2$	C_2H_2
Si_2N	MgO	KH	C_2H_4
SiC	MgOH	KCN	C_2N
Ti	MgH	$(KCN)_2$	C_3
TiO	$Mg(OH)_2$	H_2	NH_3
TiO_2	MgN	H_2O	N_2H_4
Al	Ca	HO_2	O_3
Al_2O	CaO	OH	
AlO	CaOH	H_2O_2	

$$\sqrt{\frac{K_{10} a_{Na_2SiO_3}}{a_{SiO_2} P_O}} + \sqrt{\frac{K_{11} a_{Na_2SiO_3} P_{H_2O}}{a_{SiO_2}}} + \cdots = P_{Na}^{drop}, \tag{9}$$

where K_{10} and K_{11} are the equilibrium constants for the reactions,

$$Na_2SiO_{3(l)} \Longleftrightarrow 2Na_{(g)} + SiO_{2(l)} + O_{(g)} \tag{10}$$

and

$$Na_2SiO_{3(l)} + H_2O_{(g)} \Longleftrightarrow 2NaOH_{(g)} + SiO_{2(l)} \tag{11}$$

respectively, $a_{Na_2SiO_3}$ is the activity of Na_2SiO_3, and P_{H_2O} is the partial pressure of $H_2O_{(g)}$.

The oxygen equation is a special case. In it, vapor pressure substitutions of the form of those in Eqs. (6) and (9) are made for the partial pressures of all species of those elements derived from the droplet, and substitutions of the form of those in Eq. (5) are made for the partial pressures of all other species. Thus, for example,

$$P_{H_2O} + P_{SiO} + \cdots = P_O^{tot} \tag{12}$$

becomes

$$K_1 P_H^2 P_O + K_7 a_{SiO_2}/P_O + \cdots = P_O^{tot}, \tag{13}$$

showing that P_O, and thus f_{O_2}, is determined by both the sample and the ambient gas. Because all equilibrium constants are fixed at a given temperature, and the activities of all components are fixed at a given temperature, total pressure, bulk composition, and f_{O_2}, there is only one variable for each element i that is not derived from the droplet (the partial pressure of the monatomic species of each), and only one for each element that is derived from the droplet (P_i^{drop}). The presence of oxygen, however, introduces two variables, P_O and P_O^{drop}, requiring one more equation than the number of elements.

The additional equation expresses the fact that each metal atom in the equilibrium vapor must be balanced by a number of oxygen atoms in stoichiometric proportion to it in the condensed component from which it arose. It has the form

$$\begin{aligned} P_O^{drop} = {} & 0.5P_{Na}^{drop} + P_{Mg}^{drop} + 1.5P_{Al}^{drop} + 2P_{Si}^{drop} \\ & + 0.5P_K^{drop} + P_{Ca}^{drop} + 2P_{Ti}^{drop} + 1.5P_{Cr}^{drop} \\ & + bP_{Fe}^{drop}, \end{aligned} \tag{14}$$

which introduces a new variable, $b = (X_{Fe^{2+}} + 1.5X_{Fe^{3+}})$, in which $X_{Fe^{2+}}$ is the mole fraction of Fe^{2+} expressed as a fraction of the total moles of Fe in the condensed part of the system, including any Fe present as metal. Equations analogous to (6) and (9) are substituted for the terms on the right-hand side of Eq. (14). The oxygen equation is rearranged as

$$P_O^{drop} = P_O^{tot} - P_O^{gas}, \tag{15}$$

the expanded version of Eq. (14) is substituted for P_O^{drop} and the left-hand side of Eq. (13) is substituted for P_O^{tot}. Because the temperature and bulk chemical composition of the condensed part of the system are known, b is determined when

the f_{O_2} and bulk chemical composition of the gas are known. As MELTS contains an independent relationship that links b to temperature, f_{O_2}, and the bulk chemical composition of the condensed part of the system, sufficient constraints exist to solve the system of equations. This is accomplished by using the temperature and an initial trial value for f_{O_2} in MELTS to calculate the equilibrium phase assemblage of the sample, and initial values for the activities of all liquid components in it. Together with the f_{O_2}, these activities are used to generate initial values for the partial pressures of the monatomic species of the elements not derived from the droplet and for the values of P_i^{drop} for the other elements. The partial pressure of each monatomic species and the activity of each component are substituted into the expanded version of Eq. (15), and the mismatch between its right- and left-hand sides is zeroed to generate a new estimate of f_{O_2}. A modified equilibrium phase assemblage and modified activities are calculated by using the new estimate of f_{O_2} in MELTS, and the process is repeated until all equations are solved to within two parts in 10^{15} (machine precision), usually in less than ten iterations and requiring a total of a few seconds on a 1 GHz PowerPC G4 processor, running Mac OS X 3.

Constraining the above system of equations by MELTS and solving them in this way for a sample of a particular bulk chemical composition immersed in a gas of known temperature, initial elemental composition, and total pressure yields the equilibrium condensed phase assemblage, and the partial pressures of all species, including f_{O_2}, in that ambient gas that would be necessary to stabilize the assemblage against evaporation, i.e., their equilibrium vapor pressures. It is important to note that, just as equilibrium vapor pressures may never be achieved, the phase assemblage actually present in a sample may differ from that calculated to be at equilibrium with the gas.

3. Evaporation calculation

The reason for calculating the equilibrium vapor pressure is that it is the driving force for evaporation, as expressed by the Hertz–Knudsen equation,

$$J_i = \frac{\alpha_i (P_i^v - P_i^a)}{\sqrt{2\pi M_i RT}}, \tag{16}$$

in which $J_i, \alpha_i, M_i, P_i^v$, and P_i^a are the evaporation flux in moles cm^{-2} s^{-1}, evaporation coefficient, molecular weight, equilibrium vapor pressure, and ambient pressure of species i, respectively. The purpose here is to combine laboratory measurements of fluxes from liquids of chondrule-like compositions with vapor pressures calculated by using the above type of thermodynamic modeling for the experimental conditions in order to obtain the evaporation coefficients of Fe, Na, and K. To use the experiments for this purpose, the dominant evaporating species of each element must be able to escape freely from the surface of the liquid, requiring low total pressure. Furthermore, P_i^a must be $\ll P_i^v$, requiring the pumping rate of the vacuum system or flow rate of the furnace gas to be high enough to remove material as quickly as it is evaporated (Richter, 2004). Also, evaporating species must not be desorbed from the furnace walls, where they may have been deposited during previous experiments. All of these conditions were assumed to be satisfied in the experiments modeled in this work.

The calculation is performed in the following way for an isothermal experiment. The equilibrium phase assemblage, activities of all components, f_{O_2}, corresponding vapor pressures and volume proportions of the phases are computed as above for the initial bulk composition and mass of the sample, and surrounding gas composition. The surface area of the droplet is calculated from the sum of the volumes of all phases by assuming spherical geometry, except in the Wang et al. (2001) experiments in which the residues were ellipsoidal. Setting $P_i^a = 0$, the Hertz–Knudsen equation is written for the dominant evaporating species of each element from the silicate liquid, except for Al, Ca, Ti, and Cr, which are assumed to be inert. In each experiment, fluxes of $Fe_{(g)}$, $FeO_{(g)}$, $Mg_{(g)}$, $SiO_{(g)}$, $Na_{(g)}$, and $K_{(g)}$ were calculated for various values of their evaporation coefficients.

The total flux of Fe from the silicate liquid was divided between ferrous and ferric Fe in proportion to their respective mole fractions, assuming an equal evaporation coefficient for each. When metallic Fe was stable, the evaporation coefficient of $Fe_{(g)}$ was assumed to be 1.0 for liquid Fe and to vary from 0.93 at 1720 K to 1.0 at 1810 K for solid Fe (Tachibana, pers. commun.). Solid silicate and oxide phases were assumed not to evaporate. The areal proportions of the phases on the surface of the droplet were assumed equal to their volume proportions. The fluxes of elements from the silicate liquid were multiplied by the exposed surface area of silicate liquid and those from metallic Fe by the exposed surface area of that phase. In this way, the amount of each element removed from the droplet was calculated for an evaporation step ranging from 2 s to 5 min depending on the duration of the experiment being modeled. In all cases, composition evolution paths were unchanged when recalculated at step sizes ten times smaller than those adopted. The mass and bulk composition of the droplet were recalculated for the next evaporation step and, from these, a new equilibrium phase assemblage, new activities, new f_{O_2}, new vapor pressures, new volume proportions of phases, and new surface areas were obtained. From these results, new fluxes were calculated. The entire procedure was repeated for as many evaporation steps as required to equal the duration of each experiment. The experimentally reported variation with time of either the concentration of each element or its evaporated fraction was compared to the values computed for each assumed value of α_{Fe}, α_{Mg}, α_{SiO}, α_{Na}, and α_K, and the values yielding the best fits to the data were adopted.

Although using equal evaporation coefficients for Fe^{2+} and Fe^{3+} causes equal fractions of the two species to evaporate in each step, equilibrium phase assemblages calculated in successive evaporation steps still may have slightly different molar ratios of oxidized to reduced iron. This is

due to the fact that, although the temperature is fixed, the equilibrium Fe^{3+}/Fe^{2+} ratio and its corresponding f_{O_2} for the new bulk chemical composition will, in general, be different from the previous one. The implied change in the oxygen content of the droplet was accounted for by correcting the amount of oxygen that escaped from the droplet in the intervening evaporation step by adjusting the oxygen flux relative to its stoichiometrically calculated flux. Thus, if iron underwent reduction in a given evaporation step, all excess oxygen so produced was allowed to escape in that step, enhancing the oxygen flux. If iron was oxidized in a given step, a fraction was calculated, the numerator of which is the total moles of oxygen required to increase the molar Fe^{3+}/Fe^{2+} ratio of the droplet by the indicated amount, and the denominator of which is the total moles of free oxygen that would have otherwise evaporated in that step. This fraction was used to reduce the total oxygen flux relative to its stoichiometrically calculated value. Because this fraction cannot exceed 1, the molar Fe^{3+}/Fe^{2+} ratio of an actual sample may be lower than that of the virtual equilibrium assemblage calculated for that step in cases where the amount of evaporated free oxygen is insufficient to convert the required amount of Fe^{2+} to Fe^{3+}. The resulting divergence between real and equilibrium molar Fe^{3+}/Fe^{2+} ratios does not affect the vapor pressure calculation because the correct equilibrium assemblage and corresponding vapor pressures are calculated regardless of the input molar Fe^{3+}/Fe^{2+} ratio. The assumption of instantaneous redox equilibration is consistent with experimental observations on the difficulty of retaining primary Fe^{3+}/Fe^{2+} ratios even upon very rapid quenching, as discussed by Kress and Carmichael (1989).

Iron evaporates so quickly under the conditions of the investigated experiments that its concentration fell to zero before some experiments were completed. Because there are no FeO-free compositions in the MELTS calibration database, there is no guarantee that MELTS calculates the proper activities in FeO-free systems. Because Na and K evaporate even faster than Fe, the FeO-free compositions encountered herein lie almost entirely within the system $CaO + MgO + Al_2O_3 + SiO_2$ (CMAS). Accordingly, whenever the FeO concentration fell to zero in these experiments, modeling subsequent evaporation of the residual liquid employed the activity–composition relations for the CMAS system from Berman (1983), using methods developed by Grossman et al. (2000, 2002), and Grossman and Fedkin (2003).

4. Applications

4.1. The Hashimoto (1983) experiments

Hashimoto (1983) studied a chondrule analog whose composition is shown in Table 2. This material was sintered at 1373 K in a 1-bar gas mixture whose $P_{CO_2}/P_{H_2} = 1$, where MELTS predicts the sample would have an Fe^{3+}/Fe^{2+} ratio of 0.26. He then heated the sample in a graphite crucible in a vacuum chamber at 2273, 2173, 2073, and 1973 K, and measured the changes in FeO, MgO, and SiO_2 contents as a function of time. Prior to evaporation, the pressure in the chamber was 1.3×10^{-8} bar. Assuming that the background gas in the chamber was air, there is one mass-balance equation equivalent to Eq. (1) for each of H, O, C, and N, and an equation that sums all partial pressures to the known total pressure. Since the P_H^{gas}/P_O^{gas}, P_H^{gas}/P_C^{gas}, and P_H^{gas}/P_N^{gas} ratios are known from the relative elemental abundances in air, there are only five independent variables, P_H^{gas} and the partial pressure of the monatomic species of each element, and five equations, from which the values of $P_H^{gas}, P_O^{gas}, P_N^{gas}$, and P_C^{gas} were calculated for use in the evaporation calculation. Although the presence of both the graphite crucible and low-pressure air at these temperatures would be expected to create conditions sufficiently reducing as to stabilize metallic Fe, none was reported in the experimental run products. The reason became clear in applying the vapor pressure calculation described above to these experiments. Because P_O^{drop}/P_O^{gas} was very large, $>1.5 \times 10^3$, at all times and temperatures, the chemical potential of oxygen, represented in these calculations by the f_{O_2}, was controlled by the droplet, resulting in a molar Fe^{3+}/Fe^{2+} ratio of 0.054 at the beginning of evaporation. This is lower than the ratio that was imposed on the starting material by synthesizing it in a dense, controlled atmosphere. Although MELTS predicts that no crystalline phases form during high-temperature evaporation of material of this initial composition under these conditions, olivine was reported to have formed in the experiment at 2273 K and olivine + magnetite at the lower temperatures. These phases are interpreted here as products of quenching, during which oxidation must have been rapid.

From the beginning to the end of the experiment at each temperature, calculations show that P_{Mg} and P_{SiO} are each more than 20× higher than the vapor pressure of the next most abundant gaseous species of Mg and Si, respectively. On the other hand, the P_{Fe}/P_{FeO} ratio ranges from only 3.4

Table 2
Starting compositions for experiments investigated in this work (wt.%)

	1	2	3	4	5
Na_2O	—	—	—	2.75	1.22
MgO	24.08	26.1	32.6	21.25	24.09
Al_2O_3	3.26	2.90	3.34	3.56	2.89
SiO_2	35.19	36.2	40.6	52.36	34.63
K_2O	—	—	—	3.21	0.16
CaO	2.54	2.27	2.70	0.81	1.86
TiO_2	—	0.11	0.15	0.2	0.07
Cr_2O_3	—	—	—	0.32	—
MnO	—	—	—	0.36	—
FeO	34.94	32.4	20.6	13.91	20.55
Fe	—	—	—	—	14.53
ΣREE_2O_3	—	0.17	0.20	—	—
Total	100.01	100.15	100.19	98.73	100.00

Sources: 1, Hashimoto (1983); 2, Wang et al. (2001), 2073 K; 3, Wang et al. (2001), 2273 K; 4, Yu et al. (2003), composition 1.5, Cohen et al. (2004).

at the beginning of the 2273 K experiment to 5.8 at the end, and from 4.7 to 10.2 at 1973 K. This means that, while the effect of minor gaseous species of Mg and Si on the evaporation rates of these elements can safely be ignored, the effect of $FeO_{(g)}$ on the evaporation rate of Fe cannot. In the following calculations, evaporation coefficients determined for the predominant gaseous species of each element are arbitrarily assigned to all of the minor species as well. The effect of varying α_{FeO} on the value of α_{Fe} is explored later.

The fraction of each of MgO, SiO_2, and FeO evaporated in the Hashimoto (1983) experiments is plotted as a function of time at 1973, 2073, 2173, and 2273 K in Figs. 1A–D, respectively. In these figures, both the measured and predicted total iron contents are expressed as FeO. Model curves were calculated for various sets of evaporation coef-

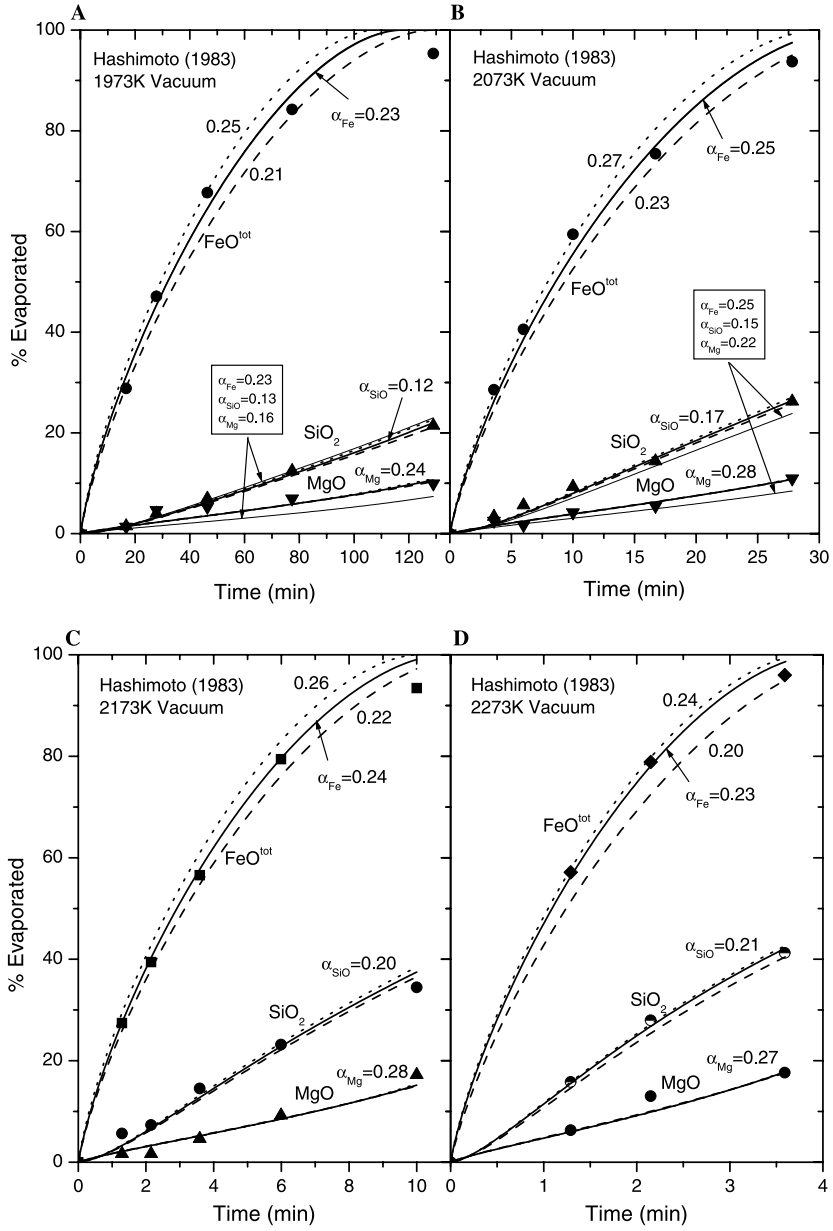

Fig. 1. Evaporation rate data (individual points) for MgO, SiO_2, and FeO from the vacuum experiments of Hashimoto (1983), compared to model predictions for the best-fit values of α_{Mg} and α_{SiO}, and three values of α_{Fe} at (A) 1973 K; (B) 2073 K; (C) 2173 K; and (D) 2273 K. Each line pattern (dashed, solid, and dotted) corresponds to a given α_{Fe}, as indicated. Note the effect of α_{Fe} on the fit to the SiO_2 data. For comparison with other data, model curves are shown for the poorer fitting pairs of $\alpha_{Mg} = 0.16$ and $\alpha_{SiO} = 0.13$ in (A), and of $\alpha_{Mg} = 0.22$ and $\alpha_{SiO} = 0.15$ in (B). All Fe is calculated as FeO, designated FeO^{tot}.

ficients to find those that best fit the experimental data plotted either as % evaporated or as wt% versus time. The method used in modeling the Hashimoto (1983) data is illustrative of that used for all experiments considered in this work. By visual means, it was found by trial and error that the fit to the data for a given element is determined predominantly by the evaporation coefficient for that element, and only very slightly by those of the other elements. Typically, the largest inter-element sensitivity is the effect of α_{Fe} on the model curves for MgO and SiO_2. After using visual means to find the set of evaporation coefficients which produce the model curves that most closely fit the experimental data, additional model curves were generated by varying the evaporation coefficient for each element by small amounts on either side of its best-fitting value, while holding constant the evaporation coefficients for the other elements. The error bars on each evaporation coefficient are the maximum deviations that still produce model curves whose fits to the data points are visually no worse than the best-fitting curves. The three curves drawn through the FeO^{tot} data in each of Figs. 1A–D are illustrative of this technique and establish that the uncertainty in α_{Fe} is ± 0.02. Also shown in these figures is the relatively small effect of this variation of α_{Fe} on the model curves drawn for the best-fitting values of α_{Mg} and α_{SiO}. The uncertainties on α_{Mg} and α_{SiO} are ± 0.01.

Evaporation coefficients obtained for $Fe_{(g)}$, $Mg_{(g)}$, and $SiO_{(g)}$ by our modeling of the Hashimoto (1983) data are summarized in Table 3, where they are compared with those derived from the same experimental data by the EQR model of Alexander (2002, 2004). Agreement is generally very good, except that our values are significantly lower than Alexander's for $Fe_{(g)}$ at 2273 K. In his application of the MELTS model to the Hashimoto (1983) experiments, Ebel (2005) found that α_{Fe} averages 0.19 ± 0.06. For each temperature, our best estimate of α_{Fe} falls within this range. Our data for $Fe_{(g)}$ and $Mg_{(g)}$ show no systematic temperature dependence, but those for $SiO_{(g)}$ show a progressive increase with increasing temperature, as do Alexander's.

Progressive changes in equilibrium vapor pressures and in the chemical composition of the sample used in the Hashimoto (1983) experiment, calculated from the evaporation model using the coefficients determined here, are illustrated in Fig. 2. The equilibrium f_{O_2} and molar Fe^{3+}/Fe^{2+} ratio are plotted in the upper panel and the corresponding equilibrium vapor pressures of $Fe_{(g)}$, $FeO_{(g)}$, $Mg_{(g)}$, and $SiO_{(g)}$ in the lower panel, all against the FeO content, in Fig. 2A at 1973 K and in Fig. 2B at 2273 K. In Fig. 2A, it is seen that $\log f_{O_2}$ fell during the experiment at 1973 K, from IW + 1.97 to IW + 1.31, where IW + x indicates an oxygen fugacity x log units above that of the iron–wüstite (IW) buffer. The equilibrium molar Fe^{3+}/Fe^{2+} ratio at the beginning of evaporation was 0.054, requiring that the starting material, whose Fe^{3+}/Fe^{2+} ratio was 0.26, underwent reduction. Even as the f_{O_2} fell during evaporation, the molar Fe^{3+}/Fe^{2+} ratio rose to 0.072 due to large changes in the bulk composition of the droplet, especially the total iron content, whose effect on the Fe^{3+}/Fe^{2+} activity ratio in the liquid offset that of the f_{O_2}. In this experiment, the amount of free oxygen evaporated was more than sufficient to produce the equilibrium Fe^{3+}/Fe^{2+} ratio required in each step. As evaporation proceeded, the corresponding P_{Fe} fell gradually from $\sim 10^{-5}$ to below 10^{-6} bar, P_{SiO} rose sharply from 2.4×10^{-7} at the beginning of the experiment and reached $\sim 3 \times 10^{-6}$, and P_{Mg} hovered around 4×10^{-7}. At 2273 K, the range of the molar Fe^{3+}/Fe^{2+} ratios was similar to that at 1973 K but the range of f_{O_2} shifted downward, to IW + 1.66 to IW + 1.20, and the range of vapor pressures shifted upward by about two orders of magnitude.

Figs. 1 and 2 were constructed assuming that evaporation coefficients of all Fe-bearing gas species are identical to that of $Fe_{(g)}$. The actual values of their evaporation coefficients have very little effect on α_{Fe} provided all other Fe-bearing species have low abundances relative to that of $Fe_{(g)}$ but, as seen above, this is not the case for $FeO_{(g)}$. The exercise of fitting the curves in Figs. 1A–D was repeated for each of a set of assumed values of α_{FeO}, 0.01, 0.1, 0.3, 0.4, and 0.5, and the effect on the value of α_{Fe} is shown in Fig. 3. As would be expected, when the value of α_{FeO} increases at a given temperature, the value of α_{Fe} necessary to fit the Fe curve at that temperature decreases. Also as expected, because P_{Fe}/P_{FeO} is always $\geqslant 3.4$, a rather large change in α_{FeO} is needed to make a significant change in α_{Fe}. The fits to the MgO and SiO_2 curves are unaffected by the value of α_{FeO}, because the fit to the FeO curve is equally good for all α_{Fe}–α_{FeO} pairs in Fig. 3. At each temperature, decreasing α_{FeO} to zero increases α_{Fe} by no more than 0.04, and increasing α_{FeO} to 0.5 decreases α_{Fe} by no more than 0.05, relative to the value of α_{Fe} given in Table 3 for the case of $\alpha_{Fe} = \alpha_{FeO}$. Because evaporation coefficients $> \sim 0.3$ are unknown from silicate melts, 0.4 would be a generous upper limit to α_{FeO}, whose selection effectively limits the possible range of α_{Fe} to within ± 0.04 of the values given in Table 3. The effect of α_{FeO} on α_{Fe} was not discussed by Alexander (2002, 2004).

Table 3
Evaporation coefficients determined for the Hashimoto (1983) vacuum experiments

	1973 K		2073 K		2173 K		2273 K	
	This work	Alexander (2004)	This work	Alexander (2004)	This work	Alexander (2004)	This work	Alexander (2004)
Fe	0.23 ± 0.02	0.25 ± 0.03	0.25 ± 0.02	0.26 ± 0.04	0.24 ± 0.02	0.27 ± 0.02	0.23 ± 0.02	0.28 ± 0.01
Mg	0.24 ± 0.01	0.27 ± 0.05	0.28 ± 0.01	0.28 ± 0.05	0.28 ± 0.01	0.28 ± 0.05	0.27 ± 0.01	0.29 ± 0.03
SiO	0.12 ± 0.01	0.16 ± 0.02	0.17 ± 0.01	0.17 ± 0.02	0.20 ± 0.01	0.19 ± 0.02	0.21 ± 0.01	0.21 ± 0.02

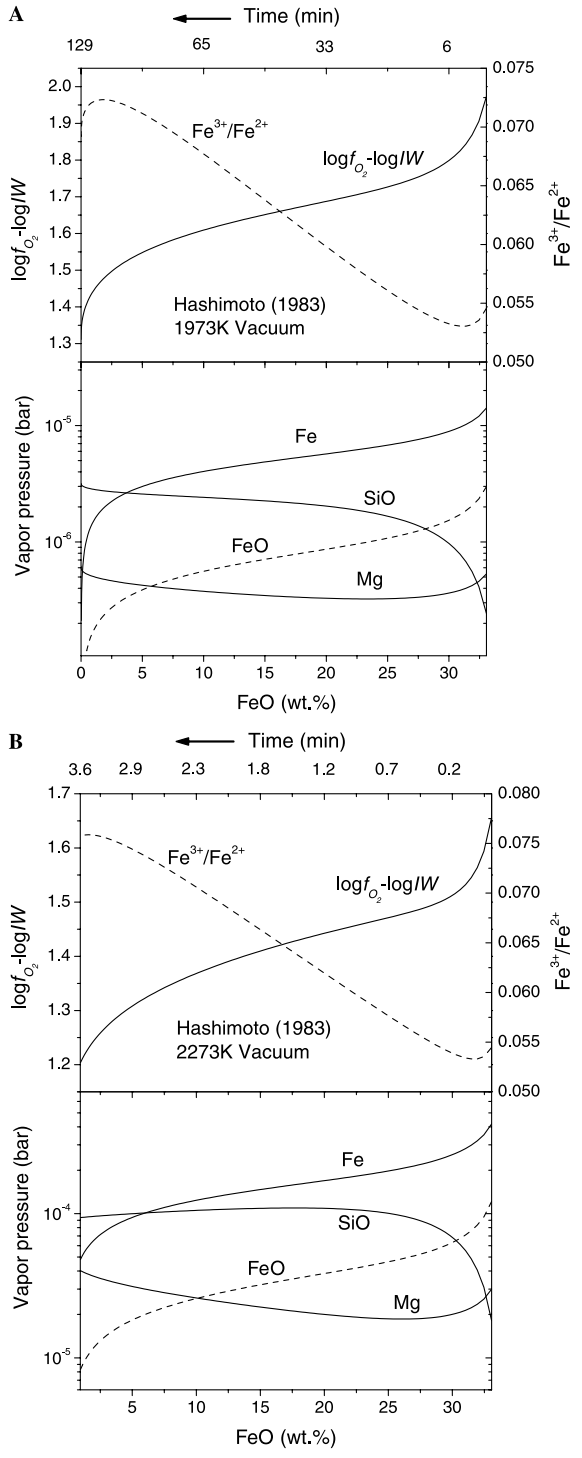

Fig. 2. Calculated oxygen fugacity relative to the iron–wüstite (IW) buffer, molar Fe^{3+}/Fe^{2+} ratio (upper panel), and equilibrium vapor pressures of $Fe_{(g)}$, $FeO_{(g)}$, $Mg_{(g)}$, and $SiO_{(g)}$ (lower panel) plotted against FeO content in the Hashimoto (1983) vacuum evaporation experiment at (A) 1973 K; and (B) 2273 K. Time-scales are shown at the tops of the figures.

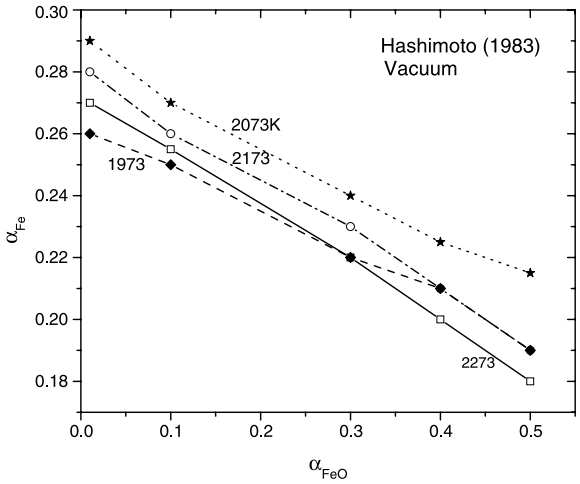

Fig. 3. Plot of α_{Fe} versus α_{FeO} for four different temperatures. Because P_{FeO} is within a factor of 10 of P_{Fe} in the Hashimoto (1983) experiments, the value obtained for α_{Fe} decreases significantly as the value adopted for α_{FeO} increases.

4.2. The Yu et al. (2003) experiments

Two chondrule analog compositions were studied by Yu et al. (2003) but only their composition 1 has sufficiently low molar K/Al to be modeled successfully by MELTS, which employs $KAlSiO_4$ as the only K-bearing component in the silicate liquid. Its composition is listed in Table 2, but MnO was ignored in our modeling. The starting material was produced by heating at 1823 K in a 1-bar CO/CO_2 mixture whose log f_{O_2} was IW − 0.5 (B.A. Cohen, pers. commun.). MELTS was used to calculate that its molar Fe^{3+}/Fe^{2+} ratio was 0.027. For this sample, the decline in the concentrations of Na_2O and K_2O was measured as a function of time at 1723 K in two sets of experiments considered here. Although orthopyroxene and/or olivine were found in the residues of both experiments, Yu et al. (2003) considered them quench products. Consequently, the olivine and orthopyroxene predicted by MELTS to crystallize at equilibrium in these experiments were suppressed in our modeling.

In the first experiment, the furnace gas was 1×10^{-5} bar air. For the evaporation calculation, P_H^{gas}, P_O^{gas}, P_N^{gas}, and P_C^{gas} were determined in the same way as for the Hashimoto (1983) experiment. The Na and K data obtained in Yu et al.'s (2003) air experiments are plotted in Figs. 4A and B, respectively, where they are compared to model calculations using three values of the evaporation coefficients for $Na_{(g)}$ and $K_{(g)}$. Because <1% of the Mg, Si, and Fe are calculated to have evaporated by the end of the experiment, the values adopted for α_{Mg}, α_{SiO}, and α_{Fe} do not affect significantly the determinations of α_{Na} and α_K. Vapor pressures of the next most abundant gaseous species of these elements, $NaO_{(g)}$ and $KO_{(g)}$, were always more than a factor of 1400 lower than for $Na_{(g)}$ and $K_{(g)}$, respectively. It is seen that the Na data are best fit by $\alpha_{Na} = 0.26 \pm 0.05$ and

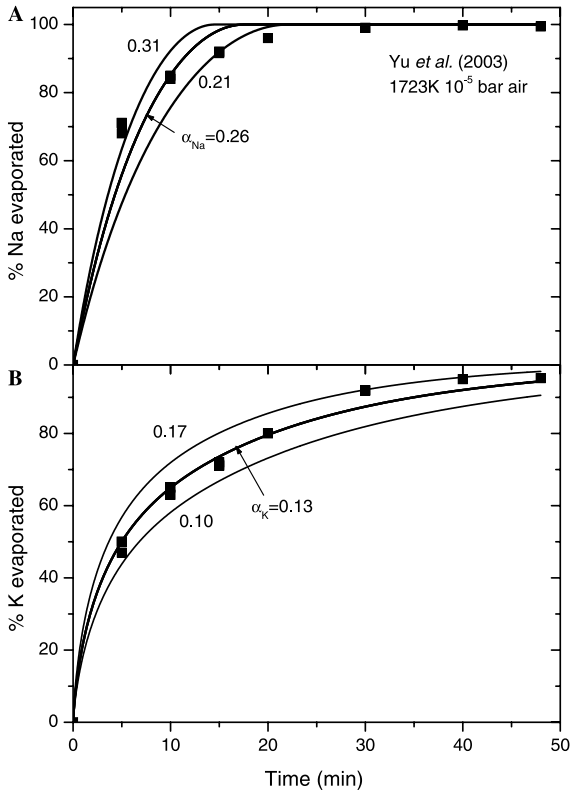

Fig. 4. Evaporation rate data for (A) Na and (B) K from the experiments of Yu et al. (2003) on a chondrule analog composition in low-pressure air, compared to predictions of the evaporation model for three values of evaporation coefficients for Na and K.

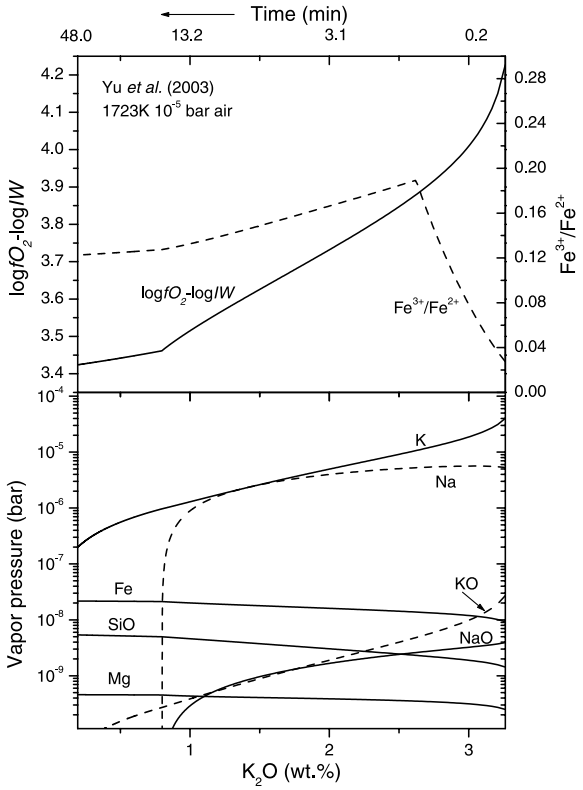

Fig. 5. Calculated equilibrium oxygen fugacity relative to IW, actual molar Fe^{3+}/Fe^{2+} ratio (upper panel) and equilibrium vapor pressures (lower panel) plotted against K_2O content in the Yu et al. (2003) evaporation experiment in low-pressure air at 1723 K. The time-scale is shown at the top of the figure.

the K data by $\alpha_K = 0.13 \pm 0.02$. Using activities from MELTS in his EQR model, Alexander (2002) modeled the same experimental data with $\alpha_{Na} = 0.12$, which is significantly lower than our value, and $\alpha_K = 0.12$, which is quite close to ours. Some of the difference between our results may come from our differing treatment of f_{O_2}. An additional source of discrepancy comes from the fact that Alexander (2002) avoided fitting those residues with the highest alkali contents, causing him to rely on those data with the largest analytical uncertainties, which may be quite severe for Na. In the present work, the residues with the highest Na contents most constrain the model curves.

The equilibrium f_{O_2} and actual molar Fe^{3+}/Fe^{2+} ratio calculated for this experiment are plotted against K_2O content in the upper panel of Fig. 5, and the equilibrium vapor pressures of the most abundant gaseous species of Na, K, Fe, Mg, and Si are plotted in the lower panel. Because the starting material had a much lower Fe^{3+}/Fe^{2+} ratio than the equilibrium value at the start of evaporation, it underwent oxidation as evaporation proceeded. For the first minute or so, however, the sample was unable to achieve the equilibrium Fe^{3+}/Fe^{2+} ratio because evaporation of alkalies provided insufficient free oxygen for it to do so. As the equilibrium $\log f_{O_2}$ fell from IW + 4.2 to IW + 3.4, the actual molar Fe^{3+}/Fe^{2+} ratio first rose to 0.19 and then fell to 0.12. Although the vapor pressure of K is initially almost an order of magnitude higher than that of Na, it is the Na which is the first to be totally volatilized. Vapor pressures of $Fe_{(g)}$, $Mg_{(g)}$, and $SiO_{(g)}$ are initially more than three orders of magnitude below that of $K_{(g)}$, making the results shown in Fig. 5 very insensitive to the evaporation coefficients for these three species and accounting for the fact that, during the course of this 48 min experiment, <1% of the Mg, Si, and Fe are lost.

In the second set of experiments, Yu et al. (2003) evacuated the furnace to 1×10^{-5} bar, then introduced hydrogen and adjusted the flow rate until the pressure was 9×10^{-5} bar. Prior to evaporation, the bulk composition of the furnace gas was assumed to consist of 9 moles of H_2 to 1 mole of air, from which $P_H^{gas}, P_O^{gas}, P_N^{gas}$, and P_C^{gas} were calculated in the same way as for the Hashimoto (1983) experiments. In the present work, equilibrium dissociation of $H_{2(g)}$ was assumed, although kinetic impediments to this reaction have been noted, as discussed by Kuroda and Hashimoto (2002). In the evaporation calculation, it was found that the equilibrium vapor pressures of $Na_{(g)}$ and $K_{(g)}$ are always larger than those of the next most

abundant gaseous species of these elements, $NaOH_{(g)}$ and $KOH_{(g)}$, by factors of >49 and >13, respectively, so evaporation coefficients of the minor species of these elements have little effect on those of $Na_{(g)}$ and $K_{(g)}$. The Na and K evaporation rate data obtained in the H_2 experiments of Yu et al. (2003) are plotted in Figs. 6A and B, respectively. Error bars on analytical data are standard deviations of multiple microprobe analyses, provided by R.H. Hewins (pers. commun.). The experimental data are compared to our model calculations for various values of the evaporation coefficients for $Na_{(g)}$ and $K_{(g)}$. In these calculations, α_{Mg}, α_{SiO}, and α_{Fe} were set equal to 0.07, 0.09, and 0.07, respectively, the same as those used for modeling the Cohen et al. (2004) H_2 experiment at a slightly higher temperature (see below). Insufficient Mg, Si, and Fe evaporated for the values adopted for α_{Mg}, α_{SiO}, and α_{Fe} to affect the determinations of α_{Na} and α_K significantly. At the end of the experiment, 0.3% of the Mg, 2.1% of the Si, and 29% of the Fe are calculated to have evaporated, but only 5% of the latter before total Na loss. It is seen that the best estimate of α_K in 9×10^{-5} bar H_2 at 1723 K is 0.017 ± 0.002. Because there are only two data points for Na at <100% evaporation and a single model curve cannot pass through both, $\alpha_{Na} = 0.042 \pm 0.020$ was obtained from the model curve passing through the data point for the least amount of Na evaporated, as this is the most accurate measurement.

The equilibrium f_{O_2} and actual Fe^{3+}/Fe^{2+} ratio calculated for this experiment are plotted against K_2O content in the upper panel of Fig. 7, and the equilibrium vapor pressures of the most abundant gaseous species of Na, K, Fe, Mg, and Si are plotted in the lower panel. As would be expected for these experiments in H_2, $\log f_{O_2}$ is lower than in air at the same temperature (Fig. 5), ranging from IW + 2.1 at the beginning of the experiment and plunging very steeply to IW − 1.6 toward the end. As a result, the initial equilibrium Fe^{3+}/Fe^{2+} ratio is not as high as in the experiment in air, and less evaporation is required to make sufficient free oxygen available for the actual Fe^{3+}/Fe^{2+} ratio to rise to the equilibrium value at 0.06. As a result of the lower f_{O_2}, the initial vapor pressures of $Na_{(g)}$, $K_{(g)}$, $Fe_{(g)}$, and $SiO_{(g)}$ are a factor of 3 or more higher than in air at the same temperature (Fig. 5). Such an effect can be deduced from the inverse relationships between vapor pressure and P_O in Eqs. (6) and (9), for example. Furthermore, because the f_{O_2} falls faster during the H_2 experiment than during the one in air, the vapor pressures

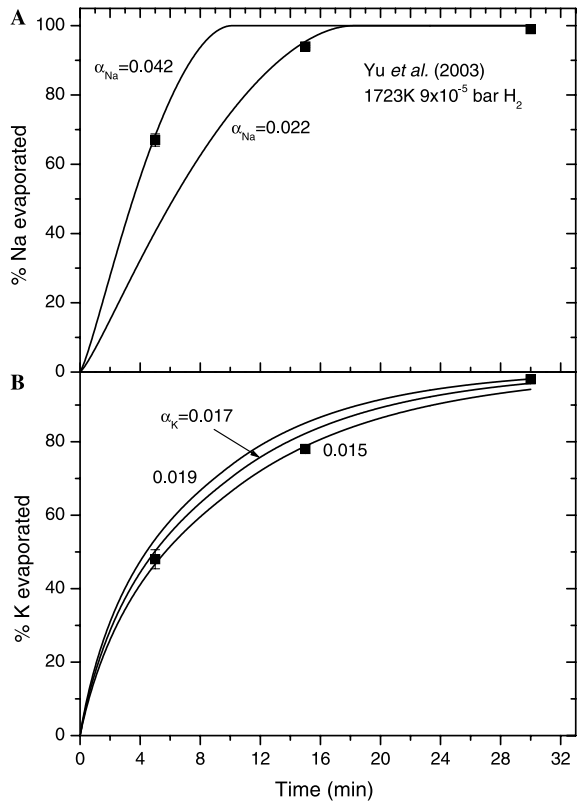

Fig. 6. Evaporation rate data for (A) Na and (B) K from the experiments of Yu et al. (2003) on a chondrule analog composition in low-pressure H_2, compared to predictions of the evaporation model for various values of evaporation coefficients for Na and K.

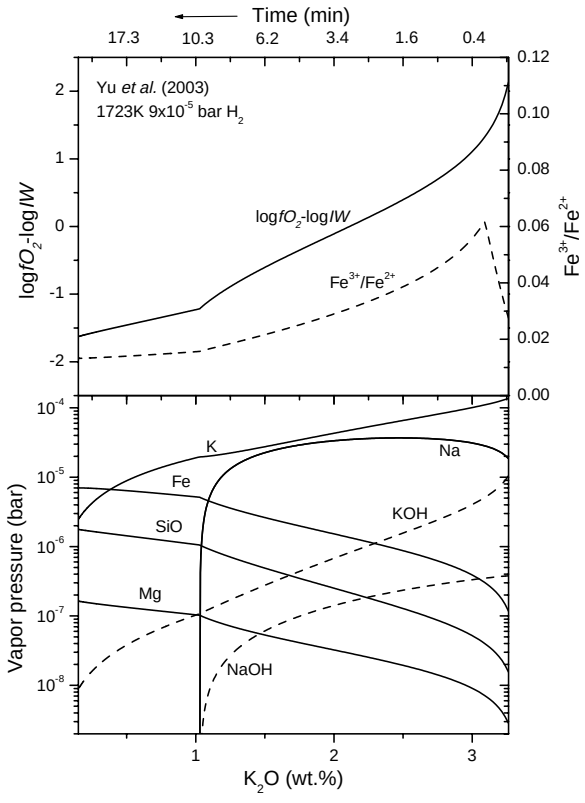

Fig. 7. Calculated equilibrium oxygen fugacity relative to IW, actual molar Fe^{3+}/Fe^{2+} ratio (upper panel) and equilibrium vapor pressures (lower panel) plotted against K_2O content in the Yu et al. (2003) evaporation experiment in H_2 at 1723 K. The time-scale is shown at the top of the figure.

of $Mg_{(g)}$, $SiO_{(g)}$, and $Fe_{(g)}$ rise more steeply than in air. After ~10 min, the rate of increase of the vapor pressures of these three species declines, in response to a simultaneous decline in the rate of decrease of the f_{O_2}. These events coincide with the sudden drop in the vapor pressure of $Na_{(g)}$ caused by the Na_2O content of the sample becoming vanishingly small. The equilibrium f_{O_2} is strongly influenced by the Fe^{3+}/Fe^{2+} activity ratio which, in these liquid compositions, decreases with decreasing Na_2O content and increases with decreasing total Fe content. Because significant Fe loss occurs after total loss of Na in this experiment, the Fe^{3+}/Fe^{2+} activity ratio, which had been falling with the K_2O content, reverses itself and begins to increase gradually with continued K loss, causing the calculated change in the variation rates of the f_{O_2} and vapor pressures.

4.3. The Wang et al. (2001) experiments

Wang et al. (2001) heated numerous samples of a S-free, REE-doped chondrule analog composition in a vacuum furnace at 20 K/min up to either 2273 or 2073 K, where they were allowed to evaporate isothermally for various time durations. The sample composition measured upon reaching each peak temperature is listed in Table 2. The composition was also measured at various elapsed times after attaining each peak temperature, up to 25 min at 2273 K and 300 min at 2073 K. For modeling purposes, these compositions were recalculated on a REE-free basis. Because of significant variations in the initial masses of the samples and because samples of different mass subjected to the same thermal history undergo different rates of chemical evolution, model results are compared only to those residues with similar initial mass. Thus, only runs SC1 through SC5, whose initial masses ranged from 160.3 to 166.3 mg, were used for modeling at 2073 K, while all 2273 K runs, whose masses ranged from 161.5 to 170.1 mg, were used. At each temperature, model curves calculated for the minimum and maximum initial masses deviated from that calculated for the average initial mass by amounts much smaller than those calculated for evaporation coefficients at the extremes of their error bars. The background pressure in the furnace was 1.3×10^{-9} bar, which is assumed here to be that of air. For the evaporation calculation, $P_H^{gas}, P_O^{gas}, P_N^{gas}$, and P_C^{gas} were determined in the same way as for the Hashimoto (1983) experiment. No crystalline phases are calculated to have reached saturation during high-temperature evaporation, so the olivine and magnetite reported by Wang et al. (2001) are interpreted here as quench products. Residue droplets in these experiments were distinctly ellipsoidal. Surface areas were provided by Davis (pers. commun.), who converted the mass of each residue to its volume at the run temperature using the density–composition relations of Lange and Carmichael (1987), and employed the diameter of the residue's Ir wire loop, corrected for thermal expansion, as two axes of the ellipsoid. Because these surface areas increase systematically with heating time by up to a factor of 2.9 relative to spheres of the same mass and composition, a regression of these surface areas against fractional mass loss was used in lieu of our usual practice of calculating surface areas assuming spherical geometry. From the start of the experiment until the time where the total Fe content falls to zero, the P_{Fe}/P_{FeO} ratio rose from 4.4 to 6.6 at 2273 K and from 4.8 to 8.5 at 2073 K. Because these ratios are relatively small, $FeO_{(g)}$ is a significant contributor to the evaporation flux of iron in this experiment.

The variation with time of the concentrations of FeO, CaO, MgO, and SiO_2 found by Wang et al. (2001) in the volatilization residues from their 2073 K experiment is shown in Figs. 8A–D, respectively, where they are compared with model evaporation curves calculated using evaporation coefficients for $Fe_{(g)}$, $FeO_{(g)}$, $Mg_{(g)}$, and $SiO_{(g)}$ determined from the Hashimoto (1983) experiment at the same temperature. For α_{FeO}, a value of 0.10 was assumed, and the corresponding value of α_{Fe}, 0.27, was taken from Fig. 3. As seen in Fig. 8A, use of these values adequately describes the rapid evaporation of Fe, whose total concentration falls to zero after 34 min. After this time, the composition was recalculated on a TiO_2-free basis and the system was modeled using the Berman (1983) activity–composition relations for the CMAS system in the manner described above. In Figs. 8B–D, data from the FeO-free stage of the experiment are compared to model results for three different pairs of evaporation coefficients for $Mg_{(g)}$ and $SiO_{(g)}$. One pair, $\alpha_{Mg} = 0.28$ and $\alpha_{SiO} = 0.17$, is the same as that used both in the MELTS modeling of the FeO-bearing stage of the same experiment and in the Hashimoto (1983) experiment at the same temperature. When these data are used, the model curves miss the experimental data points by wide margins, suggesting that evaporation coefficients for these species are different in FeO-bearing and FeO-free systems. The second pair, $\alpha_{Mg} = 0.17$ and $\alpha_{SiO} = 0.17$, was determined at 2073 K by Richter et al. (2002) in vacuum evaporation of CMAS liquids containing <15 wt% MgO. Using these data, the evaporation curves lie closer to the experimental data but still miss them by wide margins, suggesting that evaporation coefficients for these species, especially that of $SiO_{(g)}$, are significantly different in these relatively MgO-rich liquids than in the compositions investigated by Richter et al. (2002). The final pair, $\alpha_{Mg} = 0.14 \pm 0.01$ and $\alpha_{SiO} = 0.07 \pm 0.01$, provides a very good fit to the data and was obtained by trial and error. Because relatively small fractions of the MgO and SiO_2 evaporated in the Hashimoto (1983) experiment at 2073 K, the values of α_{SiO} and especially α_{Mg} obtained from that experiment may have larger uncertainties than the error in obtaining the best fits. To see if values of α_{SiO} and α_{Mg} compatible with the Hashimoto (1983) experiment could be close to those required in the FeO-free stage of the Wang et al. (2001) experiment, model curves were computed for the smallest values of these parameters that would still yield acceptable descriptions of the data in the former experiment. Such curves are shown in Fig. 1B,

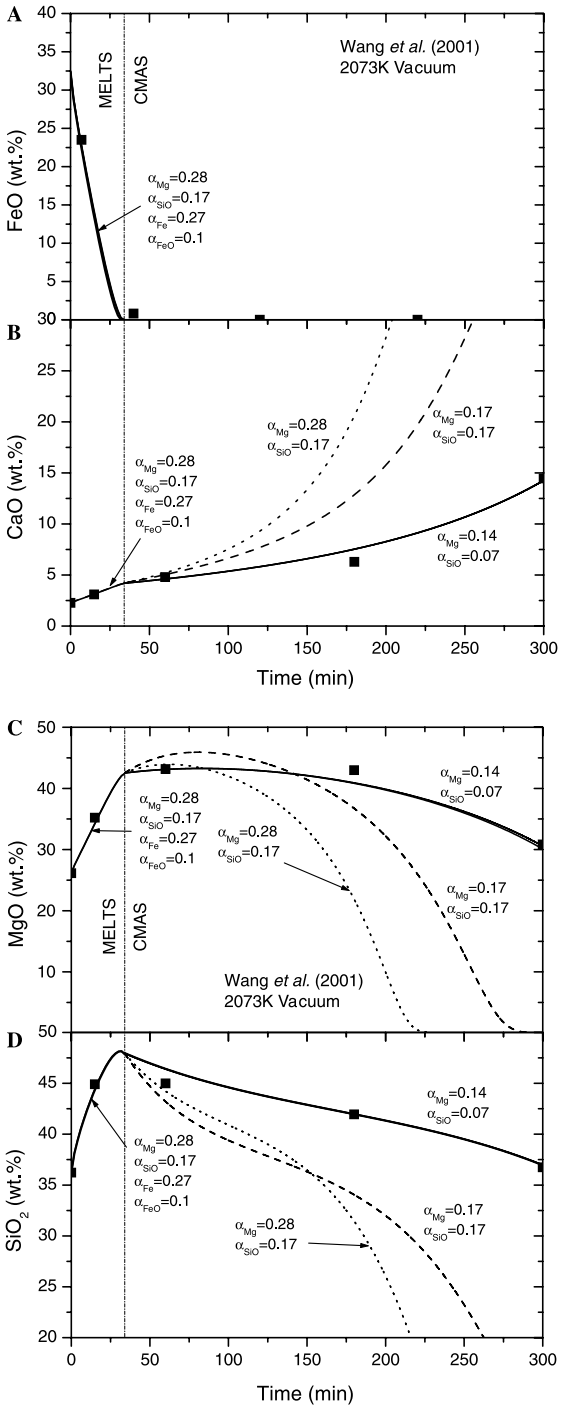

Fig. 8. Variation of the content of (A) FeO; (B) CaO; (C) MgO; and (D) SiO_2 with time in the vacuum evaporation experiments conducted by Wang et al. (2001) at 2073 K. Experimental stages modeled with MELTS and with CMAS are separated by the vertical line. In the time interval after FeO is totally evaporated, data are compared to model evaporation curves for three pairs of α_{Mg} and α_{SiO}. One pair is the same as used in MELTS modeling of the experiment prior to total FeO loss; another (0.17, 0.17) is taken from the experimental CMAS data of Richter et al. (2002); and the other is the best estimate determined here.

based on $\alpha_{Mg} = 0.22$ and $\alpha_{SiO} = 0.15$. These values give very poor fits to the data for the FeO-free stage in Fig. 8.

The starting material was sintered in the vacuum furnace at 1273 K. From this information, its molar Fe^{3+}/Fe^{2+} ratio is calculated to have been 0.22. The time variation of the equilibrium f_{O_2} and molar Fe^{3+}/Fe^{2+} ratio corresponding to the best fit curves in Fig. 8 are shown in Fig. 9A and that of the vapor pressures of $Fe_{(g)}$, $FeO_{(g)}$, $Mg_{(g)}$, and $SiO_{(g)}$ in Fig. 9B. The Fe^{3+}/Fe^{2+} ratio at the beginning of evaporation is seen to be 0.054, requiring reduction of the starting material. As log f_{O_2} falls from IW + 1.75 at the beginning of the experiment to IW + 1.25 when the iron is totally lost, the molar Fe^{3+}/Fe^{2+} ratio increases to 0.070, responding more to the sharp drop in the total Fe content than to that of the f_{O_2} (as was also the case in the Hashimoto (1983) experiment, see above). The amount of free oxygen evaporated was more than sufficient to increase the Fe^{3+}/Fe^{2+} ratio to the equilibrium value required in each step. During Fe loss, P_{Fe} falls monotonically from 4×10^{-5} bar, P_{SiO} increases from 3.0×10^{-6} to 1.2×10^{-5}, while P_{Mg} first falls from 2.0×10^{-6} to 1.5×10^{-6} and then rises to 3.0×10^{-6}. During the remainder of the experiment, P_{SiO} and f_{O_2} fall very gently and P_{Mg} rises very gently with time.

In Figs. 10A–D, data from the FeO-bearing stage of Wang et al.'s (2001) 2273 K experiment are compared with model calculations using evaporation coefficients based on

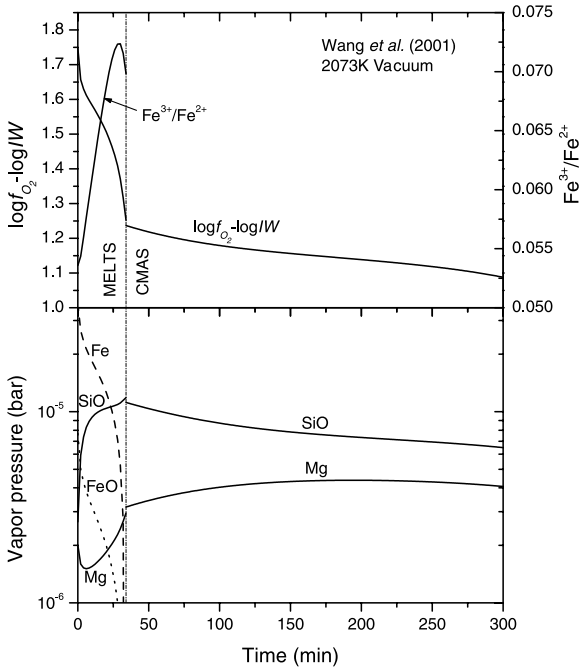

Fig. 9. Calculated equilibrium oxygen fugacity relative to IW, molar Fe^{3+}/Fe^{2+} ratio (upper panel) and vapor pressures of $Fe_{(g)}$, $FeO_{(g)}$, $Mg_{(g)}$, and $SiO_{(g)}$ (lower panel) plotted against time for the Wang et al. (2001) vacuum evaporation experiment at 2073 K. Experimental stages modeled with MELTS and with CMAS are separated by the vertical line.

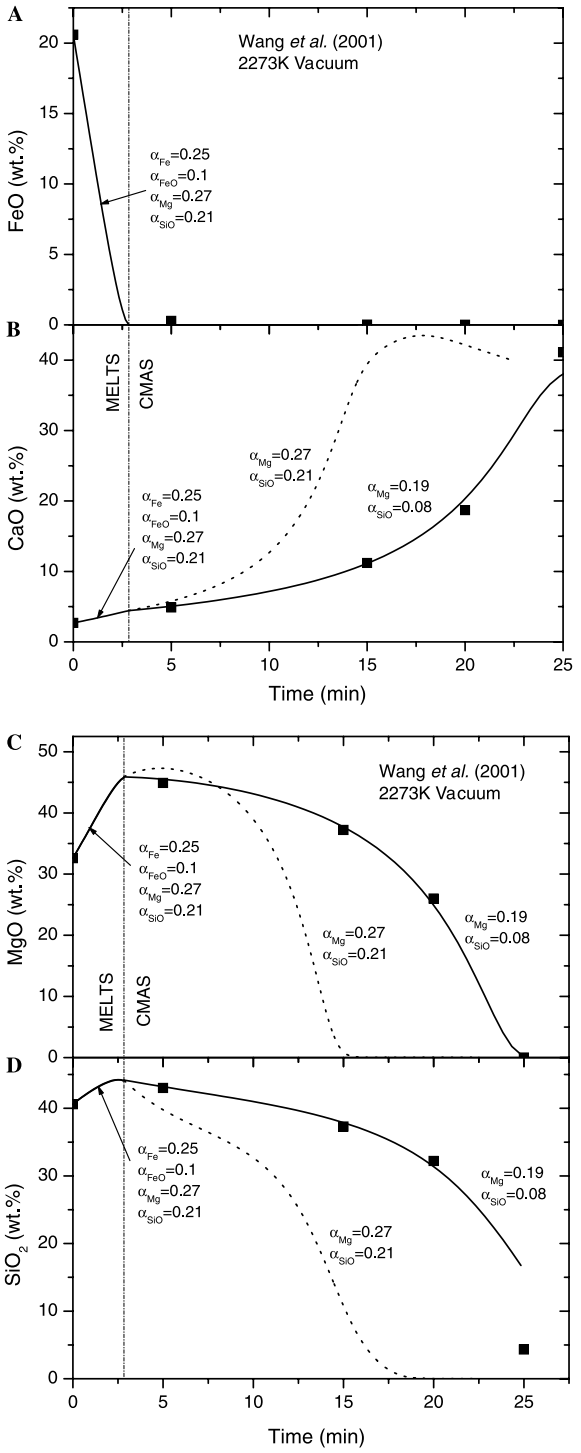

Fig. 10. Variation of the contents of (A) FeO; (B) CaO; (C) MgO; and (D) SiO_2 with time in the vacuum evaporation experiments conducted by Wang et al. (2001) at 2273 K. Experimental stages modeled with MELTS and with CMAS are separated by the vertical line. In the time interval after FeO is totally evaporated, data are compared to model evaporation curves for two pairs of α_{Mg} and α_{SiO}. One is the same as used in MELTS modeling of the experiment prior to total FeO loss, and the other is the best estimate determined here.

the Hashimoto (1983) experiment at the same temperature. Using $\alpha_{FeO} = 0.1$ and the corresponding value of α_{Fe}, 0.25, from Fig. 3, total Fe is calculated to have reached zero concentration within 3 min (Fig. 10A), after which the system was modeled using the CMAS activity model. In the FeO-free stage, experimental data for MgO, SiO_2, and CaO are compared to model predictions for two pairs of values of α_{Mg} and α_{SiO}, one derived from the Hashimoto (1983) experiment, which gives very poor fits to the data, and the other found by trial and error to give the best fits to the data. Even for the latter pair, $\alpha_{Mg} = 0.19 \pm 0.01$ and $\alpha_{SiO} = 0.08 \pm 0.01$, model curves miss the SiO_2 and CaO contents of the most evaporated residue by wide margins. As seen in Fig. 11, upper panel, the equilibrium f_{O_2} is slightly lower at 2273 K than at 2073 K (Fig. 9, upper panel), and vapor pressures of $Fe_{(g)}$, $FeO_{(g)}$, $Mg_{(g)}$, and $SiO_{(g)}$ at 2273 K (Fig. 11, lower panel) are $\sim$ an order of magnitude higher than at 2073 K.

P_{Mg}, P_{SiO}, and f_{O_2} are calculated from the MELTS model in the FeO-bearing stage of the experiment and from the CMAS model in the FeO-free stage. One measure of the incompatibility of the activity models is the magnitude of the discrepancy in each of these variables between the last evaporation step of the FeO-bearing stage and the first evaporation step of the FeO-free stage. Inspection of Figs. 9 and 11 shows that these discrepancies are small. At 2073 K, P_{Mg}, P_{SiO}, and f_{O_2} in the MELTS model are 2.96×10^{-6}, 1.19×10^{-5}, and 6.00×10^{-6}, respectively, only

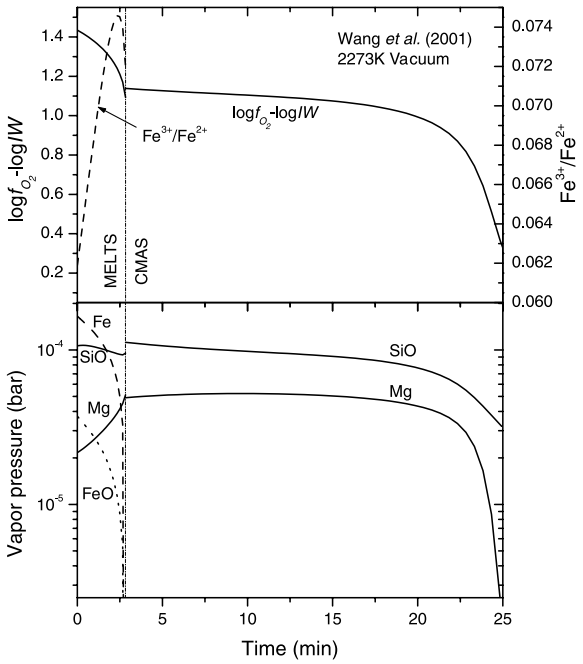

Fig. 11. Calculated equilibrium oxygen fugacity relative to IW, molar Fe^{3+}/Fe^{2+} ratio (upper panel) and vapor pressures of $Fe_{(g)}$, $FeO_{(g)}$, $Mg_{(g)}$, and $SiO_{(g)}$ (lower panel) plotted against time for the Wang et al. (2001) vacuum evaporation experiment at 2273 K. Experimental stages modeled with MELTS and with CMAS are separated by the vertical line.

6.4% lower, 6.3% higher, and 3.6% higher than their respective values in the CMAS model. Similarly, at 2273 K, P_{Mg}, P_{SiO}, and f_{O_2} in the MELTS model are only 4.3% higher, 14.9% lower, and 10.1% lower than in the CMAS model. From the functional relationship of each of P_{Mg} and P_{SiO} on f_{O_2} in the MELTS model, P_{Mg} and P_{SiO} in the latter model can be corrected to the same f_{O_2} as in the CMAS model in order to compare more directly their values to those in the CMAS model. After doing so, the corrected P_{Mg} and P_{SiO} become 5.0% lower and 8.0% higher than their respective values in the CMAS model at 2073 K; and 1.0% lower and 23.9% lower at 2273 K.

The question arises as to whether the differences in α_{Mg} and α_{SiO} inferred above for FeO-bearing and FeO-free systems are real, or artifacts of these small calibration differences between the different activity–composition models used for the two systems. Using the uncorrected vapor pressures to assess their effect on derived evaporation coefficients, α_{Mg} would have to drop in the FeO-free relative to the FeO-bearing stage by 7.3%, to 0.26, and α_{SiO} would have to increase by 5.7%, to 0.18, to preserve flux continuity at 2073 K. The actual best-fitting values of α_{Mg} and α_{SiO} for the FeO-free stage of the experiment, 0.14 and 0.07, respectively, are quite different from these values. Similarly, in Fig. 11, α_{Mg} would have to increase by 4.0% and α_{SiO} would have to drop by 17% upon entering the CMAS stage at 2273 K. The best-fitting value of α_{Mg} in the FeO-free stage of the experiment is 0.19, 30% lower than in the FeO-bearing stage, however, not 4% higher; and that of α_{SiO} is 0.08, 62% lower than in the FeO-bearing stage, rather than 17% lower. Because the best-fitting values of the evaporation coefficients differ between the stages of the experiments modeled with MELTS and those with CMAS by more than can be accounted for by calibration differences between activity models, the differences in evaporation coefficients between FeO-bearing and FeO-free systems appear to be real.

In Table 4, the values of α_{Mg} and α_{SiO} obtained here for the FeO-free stage of the Wang et al. (2001) experiments are compared with those estimated from the same experimental data by Alexander (2001) using his EQR model. The evaporation coefficients derived for both species in this work are substantially smaller than those obtained by Alexander (2001) at 2073 K. At 2273 K, however, the value obtained here for α_{Mg} is slightly larger than in that study, while that for α_{SiO} is the same. Because Alexander (2001) did not present error bars for his estimates, it is not known whether these are significant differences. Discrepancy between our values and those obtained by Alexander may be due to different ways of estimating the surface areas of the droplets, and to the fact that Alexander (2001) fitted plots of concentration versus fractional mass loss, while the more demanding task of fitting plots of concentration versus time was undertaken in the present study.

Table 4
Evaporation coefficients derived from the FeO-free portion of the Wang et al. (2001) experiments

	2073 K		2273 K	
	This work	Alexander (2001)	This work	Alexander (2001)
Mg	0.14 ± 0.01	0.19	0.19 ± 0.01	0.16
SiO	0.07 ± 0.01	0.11	0.08 ± 0.01	0.08

4.4. The Cohen et al. (2004) experiment

Cohen et al. (2004) prepared a CI-like bulk composition by pressing a mixture of olivine, diopside, plagioclase, troilite, and kerogen into pellets. Because Fe^{3+} is not an essential constituent of any of the ingredients, and because the pellets were not sintered before undergoing evaporation, it is likely that the initial Fe^{3+}/Fe^{2+} ratio of this material was very low. Cohen et al. (2004) measured its change in composition upon heating at 1853 K in 1.3×10^{-5} bar H_2 for various time durations up to 18 h. C, S, Na, and K were totally lost in the first hour, before the first residue was sampled in these experiments. The starting composition for our modeling is given in Table 2. It was derived from the one given by Cohen et al. (2004) by subtracting all C, S, and MnO, and considering all Fe associated with FeS to be present as Fe. Before introduction of H_2, the pressure in the furnace was 1.3×10^{-7} bar, so the ambient gas was treated as a mixture of 99 parts H_2 and one part air in our modeling. Values of P_H^{gas}, P_O^{gas}, P_N^{gas}, and P_C^{gas} were calculated as in the treatment of the Hashimoto (1983) data, again assuming that there was no kinetic impediment to dissociation of $H_{2(g)}$ in these experiments. It should be noted that, in this experiment, samples heated for different times differed so much from one another in initial mass that each had to be modeled separately to find the best values of evaporation coefficients. The model curves shown in Fig. 12 are for a hypothetical sample of the average initial mass.

The changes in concentration of FeO, CaO, MgO, and SiO_2 with heating time measured by Cohen et al. (2004) are illustrated in Figs. 12A–D, respectively, where they are compared with model evaporation curves based on a very low assumed initial molar Fe^{3+}/Fe^{2+} ratio of 0.005. Results for a higher initial ratio of 0.015 are discussed later. No estimates of uncertainty were provided by Cohen et al. (2004) for the bulk composition measurements. Because FeO was totally lost between 6 and 12 h after the start of this experiment, modeling was performed in two stages: an initial, FeO-bearing one treated with the MELTS activity model, and an FeO-free stage with the CMAS model, after recalculating the composition on a TiO_2-free basis. When the initial stage is run for the full duration of the experiment, however, the FeO content does not actually reach zero but only approaches it asymptotically. The rate of decline of the FeO content becomes very low at ~0.07 wt% at 10 h, and this time was taken to define the boundary between the two stages. For the initial stage, an attempt was made to fit the experimental data using evaporation coefficients derived from the Hashimoto (1983) experiment. To correct for temperature, the data in Table 3 were extrapolated linearly to 1853 K

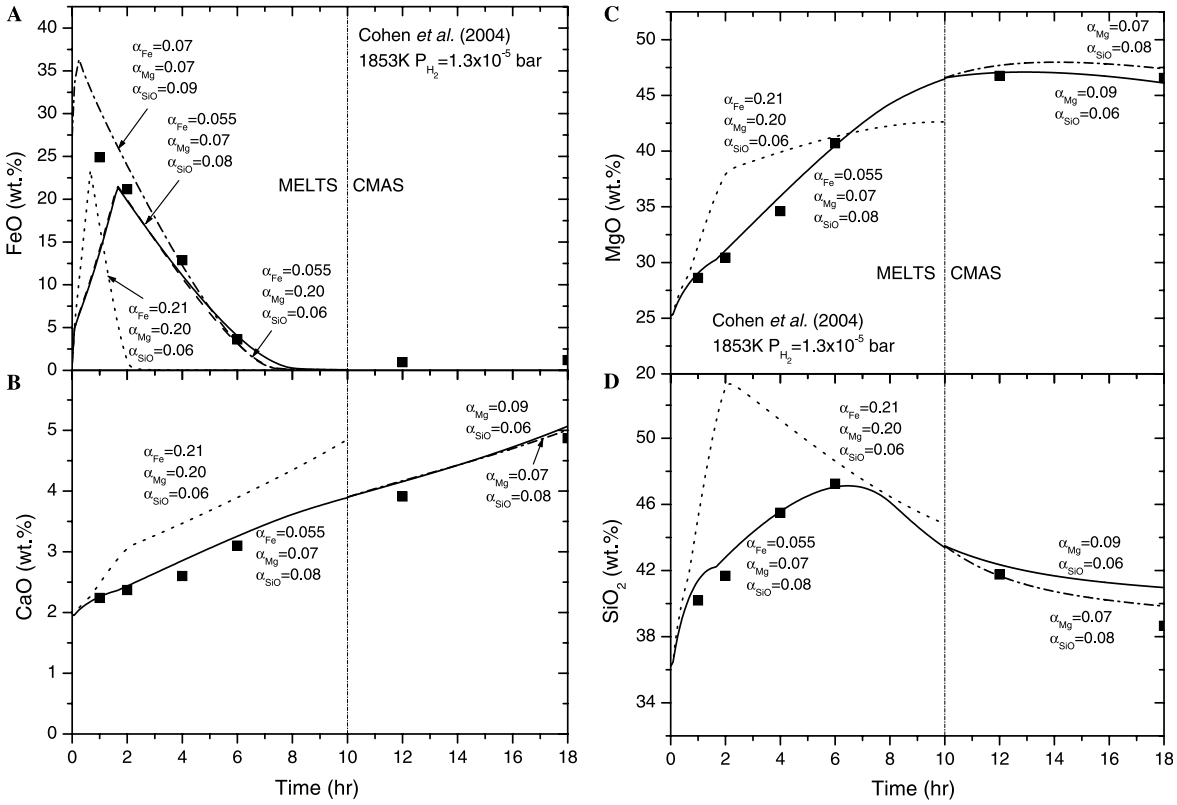

Fig. 12. Variation of concentrations of (A) FeO; (B) CaO; (C) MgO; and (D) SiO_2 with heating time in the evaporation experiments of Cohen et al. (2004) on a chondrule analog composition in 1.3×10^{-5} bar H_2 at 1853 K, compared to model predictions for various values of the evaporation coefficients. In (A), all model curves are calculated for an initial molar Fe^{3+}/Fe^{2+} ratio of 0.005, except for the dash-dot curve for which this ratio is 0.015. Experimental stages modeled with MELTS and with CMAS are separated by the vertical line. Very poor fits (dotted curves) to the FeO and SiO_2 data are obtained using values of α_{Fe} and α_{SiO} extrapolated to this temperature from those used to model the Hashimoto (1983) vacuum experiments.

using a log α versus 1/T equation. For this purpose, the data for each of α_{Fe} and α_{Mg} in Table 3 were considered uniform at 2073 K and above, so only the two lowest temperature values were used for extrapolation of these data. Using the data so obtained, $\alpha_{Fe} = 0.21$, $\alpha_{Mg} = 0.20$, and $\alpha_{SiO} = 0.06$, along with the values of α_{Na} and α_K taken from the Yu et al. (2003) hydrogen experiment, FeO is predicted to evaporate much more quickly than observed experimentally (Fig. 12a), and very poor model fits also result for the CaO, MgO, and SiO_2 data in Figs. 12B–D. By trial and error, it was found that the experimental data are best fit when $\alpha_{Fe} = 0.055 \pm 0.010$, $\alpha_{Mg} = 0.07 \pm 0.05$, and $\alpha_{SiO} = 0.08 \pm 0.01$, and the values of α_{Na} and α_K remain the same. Model curves are also shown for this set of data in each of Figs. 12A–D. Another model curve, constructed with $\alpha_{Fe} = 0.055$, the same values of α_{Na} and α_K, and the values of α_{Mg} and α_{SiO} extrapolated from the Hashimoto (1983) experiment, is shown in Fig. 12A. It shows how insensitive the determination of α_{Fe} is to the values adopted for α_{Mg} and α_{SiO}. The P_{Fe}/P_{FeO} ratio ranges from ~13 at the beginning to ~133 at the end of the FeO-bearing stage of the experiment, so even a variation in the value of α_{FeO} from 0.01 to 0.50 produces a variation in α_{Fe} of only ± 0.01.

The value of α_{Fe} obtained here is more than a factor of three lower than the very well-determined and relatively temperature insensitive value obtained from the Hashimoto (1983) vacuum experiment at a temperature only 120 K higher than this (Fig. 1A). Assuming there were no experimental artifacts, such as a continuous supply of iron to the sample from the coatings on the Re wire loops on which the samples were suspended, this result implies that α_{Fe} is lower in H_2 than in vacuum. In the present model, the surface areal fraction of metallic iron is assumed to equal its volume fraction. If, however, crystal settling caused the areal fraction of metal to be less than this, the silicate fraction would have had to contribute more to the total measured iron evaporation rate, requiring a higher α_{Fe} than calculated. In order to see if such an effect could cause α_{Fe} for this experiment to approach the value derived from the Hashimoto (1983) experiment, an identical model calculation was performed on the Cohen et al. (2004) experiment, except that the surface area of metal was reduced by a factor of two at each step. To fit the experimental data as well as the curves shown in Figs. 12A–D, α_{Fe} had to be raised to 0.065, within the stated error bars on α_{Fe} and still a factor of three less than the value derived from the Hashimoto (1983) experiment.

Considering the uncertainties, the value of α_{SiO} that best fits the Cohen et al. (2004) experimental data in H_2 is very close to the value extrapolated from the Hashimoto (1983) vacuum experiments, but the one for α_{Mg} is not. Using the error bars to define the smallest value of α_{SiO} and the largest value of α_{Mg} compatible with the Cohen et al. (2004) data, and extrapolating these values to 1973 K, yields $\alpha_{SiO} = 0.13$ and $\alpha_{Mg} = 0.16$. Using these values in an attempt to model the SiO_2 and MgO data in the Hashimoto (1983) vacuum experiment at 1973 K yields the curves labeled with these α's in Fig. 1A. While the fits to the data are clearly poorer than the others shown in this figure, they are nevertheless permissible descriptions of the data, especially considering the relatively small amounts of MgO and SiO_2 evaporated in the Hashimoto (1983) experiment and the unknown measurement uncertainty. Thus, a comparison of the FeO-bearing stage of the Cohen et al. (2004) experiment in H_2 with the Hashimoto (1983) vacuum evaporation experiment yields no compelling reason to adopt different values of α_{Mg} and α_{SiO} in H_2 than in vacuum.

Because of the high MgO concentrations encountered in the FeO-free stage of the Cohen et al. (2004) experiment, the best values of α_{Mg} and α_{SiO} found in the FeO-free stage of the Wang et al. (2001) experiments were also used here, after extrapolating the data in Table 4 to 1853 K. It is seen that use of these values, $\alpha_{Mg} = 0.09$ and $\alpha_{SiO} = 0.06$, yields good model fits to the data for the FeO-free stages of the experiments in Figs. 12B–D. Slightly better fits are obtained when the values of α_{Mg} and α_{SiO} used to model the FeO-bearing stage of the Cohen et al. (2004) experiment are also used for the FeO-free stage. Recall that the former data are extrapolated from the higher-temperature values used to model the Hashimoto (1983) vacuum experiments.

The actual bulk Fe^{3+}/Fe^{2+} ratio and equilibrium f_{O_2} corresponding to the best-fitting model in Fig. 12 are plotted against time in the upper panel of Fig. 13, and the vapor pressures of $Fe_{(g)}$, $FeO_{(g)}$, $Mg_{(g)}$, and $SiO_{(g)}$ in the lower panel. For a sample of this initial bulk composition and assumed Fe^{3+}/Fe^{2+} ratio, the equilibrium assemblage at 1853 K consists of 45 wt% silicate liquid, 31 wt% liquid metallic Fe, and 24% olivine whose $X_{Fa} = 0.018$. Release of free oxygen that accompanied the beginning of evaporation yielded an initial equilibrium log f_{O_2} of IW + 3.7, which was the driving force for conversion of metallic Fe to FeO and Fe_2O_3. For the first 95 min, however, evaporation of alkalies and FeO provided insufficient free oxygen for the sample to achieve the equilibrium Fe^{3+}/Fe^{2+} ratio. During this time, metallic Fe disappeared, some by direct evaporation but most by oxidation, as the actual Fe^{3+}/Fe^{2+} ratio of the bulk silicate rose to 0.029 and the equilibrium log f_{O_2} fell to ~IW + 0.4. Olivine was resorbed, reaching an abundance of 15 wt% and an X_{Fa} of 0.09. After this time, the actual Fe^{3+}/Fe^{2+} ratio leveled off, then fell sharply and then gradually approached zero, as the equilibrium log f_{O_2} fell to ~IW − 0.6. Olivine increased to 60 wt% of the sample and its X_{Fa} fell to

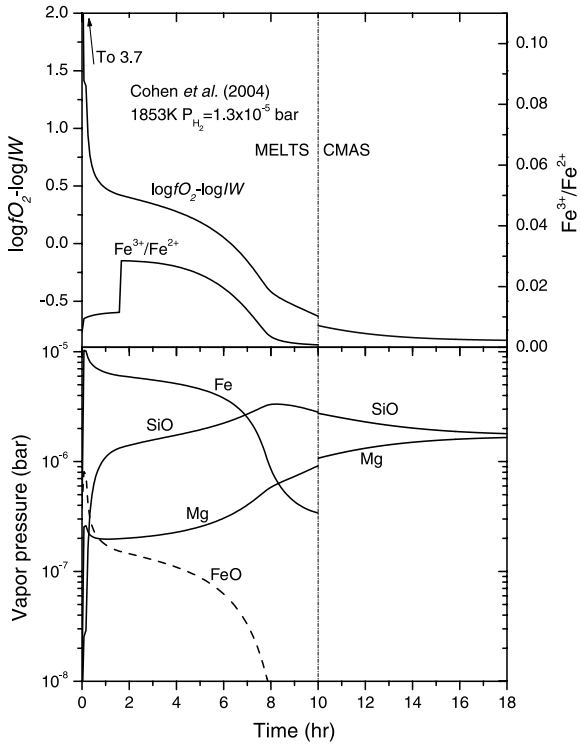

Fig. 13. Calculated oxygen fugacity relative to IW, actual molar Fe^{3+}/Fe^{2+} ratio (upper panel), and equilibrium vapor pressures of $Fe_{(g)}$, $FeO_{(g)}$, $Mg_{(g)}$, and $SiO_{(g)}$ (lower panel) plotted against time for the Cohen et al. (2004) evaporation experiment in H_2 at 1853 K. Model calculations assume an initial molar Fe^{3+}/Fe^{2+} ratio of 0.005. Experimental stages modeled with MELTS and with CMAS are separated by the vertical line.

0.001 after 10 h. It is the stabilization of this small amount of FeO in the olivine that buffers the small amount of FeO in the coexisting liquid and prevents total evaporation of FeO. In the FeO-free stage, the amount of olivine predicted with the CMAS model was lower, starting with 53 wt% at 10 h and falling to 49% at the end of the experiment. In the run products, Cohen et al. (2004) found copious olivine whose X_{Fa} varied from 0.18 after 1 h to 3.4×10^{-3} after 18 h and no spinel. In Fig. 13B, it is seen that the vapor pressures of $SiO_{(g)}$ and $Mg_{(g)}$ rise steeply as evaporation proceeds, while that of $Fe_{(g)}$ falls, leveling off at $\sim 3 \times 10^{-7}$ bar as a consequence of the slowdown in the rate of decline of the FeO content.

If, instead, a higher initial Fe^{3+}/Fe^{2+} ratio of 0.015 is assumed for the starting material, the initial contents of olivine ($X_{Fa} = 0.11$) and liquid metallic Fe are only 8 wt% and 9%, respectively. Metallic Fe disappears after 10 min, and the actual Fe^{3+}/Fe^{2+} ratio achieves its equilibrium value after 20 min, when olivine reaches $X_{Fa} = 0.12$. Minor spinel containing ~19 wt% MgO, 11% FeO, 32% Fe_2O_3, 35% Al_2O_3, and 3% TiO_2 appeared after 15 min but was stable for only 5 min in the model calculation. Despite these differences, the equilibrium vapor pressures were similar to those in the above case of lower initial Fe^{3+}/Fe^{2+} ratio, and the best fit (e.g., dash-dot curve in Fig. 12A) to the

experimental data was achieved with only slightly different values of α_{Fe} (0.07) and α_{SiO} (0.09).

5. Conclusions

Little is known about the factors that influence evaporation coefficients, and there is no theory for calculating them from first principles. In reviewing the uncertainty in α for forsterite evaporation, Tsuchiyama et al. (1999) pointed out that it varies by a factor of five with temperature, gas composition, and crystallographic orientation. In the present study, application of modern activity–composition models to chondrule analogs whose evaporation kinetics have been studied experimentally leads to the conclusion that the evaporation coefficient for a given species depends on the liquid composition and on the surrounding gas composition. It was found that, in FeO-bearing systems at constant temperature, α_{Fe}, α_{Na}, and α_{K} are significantly lower in low-pressure H_2 gas than in vacuum or low-pressure air, while α_{Mg} and α_{SiO} may be the same. It was also found that, at a given temperature, α_{Mg} and α_{SiO} are significantly lower in FeO-free systems than in FeO-bearing ones in vacuum, while they are the same in H_2. In FeO-free systems, α_{Mg} and especially α_{SiO} are significantly lower at high MgO contents (>30 wt%) than at low MgO ($\leqslant$15%) at the same temperature. Evaporation coefficients determined here will be used to predict the chemical and isotopic evolution of precursors of ferromagnesian chondrules upon melting in various nebular gas compositions.

Acknowledgments

We thank A.M. Davis for unpublished surface area data on the Wang et al. (2001) residues, B.A. Cohen for unpublished details of the Yu et al. (2003) and Cohen et al. (2004) experiments, S. Tachibana for unpublished evaporation coefficient data for solid and liquid iron, two anonymous referees for penetrating reviews, and C.M.O'D. Alexander, A.J. Campbell, R.H. Hewins, and S.B. Simon for helpful discussions. This work was supported by NASA Grants NAG5-11588 and NNG05GG00G (to L.G.), and NSF Grant EAR-0401510 (to M.S.G.), and funding is gratefully acknowledged.

Associate editor: Bjorn Mysen

References

Alexander, C.M.O'.D., 2001. Exploration of quantitative kinetic models for the evaporation of silicate melts in vacuum and in hydrogen. *Meteorit. Planet. Sci.* **36**, 255–283.

Alexander, C.M.O'.D., 2002. Application of MELTS to kinetic evaporation models of FeO-bearing silicate melts. *Meteorit. Planet. Sci.* **37**, 245–256.

Alexander, C.M.O'.D., 2004. *Meteorit. Planet. Sci.* **39**, 163, Erratum.

Alexander, C.M.O'.D., Wang, J., 2001. Iron isotopes in chondrules: implications for the role of evaporation during chondrule formation. *Meteorit. Planet. Sci.* **36**, 419–428.

Alexander, C.M.O'.D., Grossman, J.N., Wang, J., Zanda, B., Bourot-Denise, M., Hewins, R.H., 2000. The lack of potassium isotopic fractionation in Bishunpur chondrules. *Meteorit. Planet. Sci.* **35**, 859–868.

Berman, R.G., 1983. A thermodynamic model for multicomponent melts, with application to the system CaO–MgO–Al_2O_3–SiO_2. Ph.D. thesis, University of British Columbia.

Cohen, B.A., Hewins, R.H., Alexander, C.M.O'.D., 2004. The formation of chondrules by open-system melting of nebular condensates. *Geochim. Cosmochim. Acta* **68**, 1661–1675.

Ebel, D.S., 2005. Model evaporation of FeO-bearing liquids: application to chondrules. *Geochim. Cosmochim. Acta* **69**, 3183–3193.

Ebel, D.S., Grossman, L., 2000. Condensation in dust-enriched systems. *Geochim. Cosmochim. Acta* **64**, 339–366.

Fedkin, A.V., Grossman, L., Ghiorso, M.S., 2005. Vapor pressures and evaporation coefficients of Fe, Na, and K over chondrule composition melts. In: *Lunar Planetary Science*. XXXVI, Abstract #2273, Lunar and Planetary Institute, Houston (CD-ROM).

Ghiorso, M.S., Sack, R.O., 1995. Chemical mass transfer in magmatic processes IV. A revised and internally consistent thermodynamic model for the interpolation and extrapolation of liquid–solid equilibria in magmatic systems at elevated temperatures and pressures. *Contrib. Mineral. Petrol.* **119**, 197–212.

Grossman, L., Fedkin, A.V., 2003. CaO–MgO–Al_2O_3–SiO_2 liquids: chemical and isotopic effects of Mg and Si evaporation in a closed system of solar composition. *Geochim. Cosmochim. Acta* **67**, 4205–4221.

Grossman, L., Ebel, D.S., Simon, S.B., Davis, A.M., Richter, F.M., Parsad, N.M., 2000. Major element chemical and isotopic compositions of refractory inclusions in C3 chondrites: the separate roles of condensation and evaporation. *Geochim. Cosmochim. Acta* **64**, 2879–2894.

Grossman, L., Ebel, D.S., Simon, S.B., 2002. Formation of refractory inclusions by evaporation of condensate precursors. *Geochim. Cosmochim. Acta* **66**, 145–161.

Hashimoto, A., 1983. Evaporation metamorphism in the early solar nebula-evaporation experiments on the melt FeO–MgO–SiO_2–CaO–Al_2O_3 and chemical fractionations of primitive materials. *Geochem. J.* **17**, 111–145.

Hewins, R.H., Connolly, H.C., Lofgren, G.E., Libourel, G., 2005. Experimental constraints on chondrule formation. In: Krot, A.N., Scott, E.R.D., Reipurth, B. (Eds.), *Chondrites and the Protoplanetary Disk*, in press.

Jones, R.H., 1990. Petrology and mineralogy of type II, FeO-rich chondrules in Semarkona (LL3.0): origin by closed-system fractional crystallization, with evidence for supercooling. *Geochim. Cosmochim. Acta* **54**, 1785–1802.

Jones, R.H., 1994. Petrology of FeO-poor, porphyritic pyroxene chondrules in the Semarkona chondrite. *Geochim. Cosmochim. Acta* **58**, 5325–5340.

Kress, V.C., Carmichael, I.S.E., 1989. The lime–iron–silicate melt system: redox and volume systematics. *Geochim. Cosmochim. Acta* **53**, 2883–2892.

Kuroda, D., Hashimoto, A., 2002. The reaction of forsterite with hydrogen—its apparent and real temperature dependences. *Antarct. Meteorit. Res.* **15**, 152–164.

Lange, R.A., Carmichael, I.S.E., 1987. Densities of Na_2O–K_2O–CaO–MgO–FeO–Fe_2O_3–Al_2O_3–TiO_2–SiO_2 liquids: new measurements and derived partial molar properties. *Geochim. Cosmochim. Acta* **51**, 2931–2946.

Richter, F.M., 2004. Timescales determining the degree of kinetic isotope fractionation by evaporation and condensation. *Geochim. Cosmochim. Acta* **68**, 4971–4992.

Richter, F.M., Davis, A.M., Ebel, D.S., Hashimoto, A., 2002. Elemental and isotopic fractionation of type B calcium-, aluminum-rich inclusions: experiments, theoretical considerations, and constraints on their thermal evolution. *Geochim. Cosmochim. Acta* **66**, 521–540.

Tsuchiyama, A., Tachibana, S., Takahashi, T., 1999. Evaporation of forsterite in the primordial solar nebula; rates and accompanied isotopic fractionation. *Geochim. Cosmochim. Acta* **63**, 2451–2466.

Wang, J., Davis, A.M., Clayton, R.N., Mayeda, T.K., Hashimoto, A., 2001. Chemical and isotopic fractionation during the evaporation of the FeO–MgO–SiO_2–CaO–Al_2O_3–TiO_2 rare earth element melt system. *Geochim. Cosmochim. Acta* **65**, 479–494.

Yu, Y., Hewins, R.H., Alexander, C.M.O'.D., Wang, J., 2003. Experimental study of evaporation and isotopic mass fractionation of potassium in silicate melts. *Geochim. Cosmochim. Acta* **67**, 773–786.